九州大学学術情報リポジトリ
Kyushu University Institutional Repository

Computational Aerodynamic Investigations on Wash Out Twist Morphing MAV Wings

N. I. Ismail
Centre of Mechanical Engineering Studies, Universiti Teknologi MARA, Pulau Pinang Branch, Permatang Pauh Campus

M. Asyraf Tasin
Centre of Mechanical Engineering Studies, Universiti Teknologi MARA, Pulau Pinang Branch, Permatang Pauh Campus

Sharudin, Hazim
Creative and Innovation Research Group in Automotive and Aviation (CIRAA), Universiti Teknologi MARA Cawangan Pulau Pinang

M. Hisyam Basri
Centre of Mechanical Engineering Studies, Universiti Teknologi MARA, Pulau Pinang Branch, Permatang Pauh Campus

他

https://doi.org/10.5109/6625721

出版情報：Evergreen. 9 (4), pp.1090-1102, 2022-12. 九州大学グリーンテクノロジー研究教育センター
バージョン：
権利関係：Creative Commons Attribution-NonCommercial 4.0 International

KYUSHU UNIVERSITY

Computational Aerodynamic Investigations on Wash Out Twist Morphing MAV Wings

N. I. Ismail[1,2*], M. Asyraf Tasin[1], Hazim Sharudin[2,3], M. Hisyam Basri[1,2], S. Che Mat[1,2], H. Yusoff[1] & R.E.M. Nasir[4]

[1]Centre of Mechanical Engineering Studies, Universiti Teknologi MARA, Pulau Pinang Branch, Permatang Pauh Campus, 13500 Penang, Malaysia

[2]Creative and Innovation Research Group in Automotive and Aviation (CIRAA), Universiti Teknologi MARA Cawangan Pulau Pinang, 13500 Penang, Malaysia

[3]Centre of Mechanical Engineering Studies, Universiti Teknologi MARA, Johor Branch, Pasir Gudang Campus, 81750 Johor, Malaysia

[4]Flight Technology & Test Research Group (FTTC), College of Engineering, Universiti Teknologi MARA, 40450 Shah Alam, Selangor, Malaysia

*Author to whom correspondence should be addressed:
E-mail: iswadi558@uitm.edu.my

(Received July 6, 2022; Revised October 11, 2022; accepted October 26, 2022).

Abstract: Fixed-wing MAV with morphing wing configuration is seen as the future design requirements for more aerodynamic efficiency. Wash in twist morphing MAV wings have shown a promising ability by producing smoother lift behavior and exhibited a significant increase in lift performances. However, the wash in twist morphing wings also suffer from massive drag penalties as compared to rigid or membrane (baseline) wings. Thus, the objective of this paper is to explore the aerodynamic performances of another morphing configuration known as wash out twist morphing MAV wing with a view towards the improvement of the drag performances of morphing MAV wing. Technically, the wash out twist morphing (TM) wing has deformation characteristics which are opposite from those of the wash in morphing wing. The force execution of the wash out morphing wing is similar to the wash in wing but with reversed vector direction. The investigation was carried out based on Fluid-Structure-Interaction (FSI) simulation method. The simulation was conducted in a 3D, quasi-static linear structural model combined with a steady-state, incompressible, and turbulent flow model. Three levels of the wash out morphing force (5N, 3N, and 1N) were used here to evaluate the morphing performances together with the baseline wing models (membrane wing and rigid wing). The lift coefficient results show that the wash out TM wings produced inferior lift performances compared to the baseline wings. This is due to weak vortices interactions, which lead to substantial adverse pressure on the TM wings. Meanwhile, TM wings have slight advantages in producing better drag performances than the rigid and membrane wings. Vortices study discovered that the TM wings have a weak tip vortex formation, which subsequently induces lower drag magnitude. However, the drag advantages found on the TM wings are still unable to overcome the lift drawbacks, which in turn, reducing the overall aerodynamics efficiency performances.

Keywords: Wash out Twist Morphing Wing; Biomimetic Wing, Micro Air Vehicle; Aerodynamics

1. Introduction

Micro air vehicle (MAV) is a relatively new generation of aircraft. MAV design becomes a feasible aircraft design over the past 15 years due to continuous research in micro size wings. Technically, MAV is defined as a micro-scale class of Unmanned Aerial Vehicle (UAV), which has the wingspan equals to or less than 6 inches (approximately 15 cm)[1–4]. MAV velocity speed is less than 15 m/s, with the overall weight less than 1 kg[5,6] The fixed-wing MAV type is the most popular choice among researchers since the design offers better payload and endurance capability[7,8]. However, the fixed-wing MAV also suffers from several drawbacks, such as the low lift and high drag generation[9,10] It also has a nature of difficult flight controllability and a small center of gravity (CG)

range[11,12] The biological wing inspirations, such as morphing wings, have been introduced to improve the performance of fixed-wing MAV aerodynamics[13,14].

Morphing is defined as an ability of an aircraft's wing to change its shape during a flight to improve its overall flight performance[15]. It is also known as a biomimetic wing design[14] that provides a smooth and continuous wing shape changes through the feature of wing flexibility. The biomimetic morphing wing is a new generation of wing mobility adopted in micro air vehicle[16] (MAV) flight, which can be classified accordingly to the outcome of shape parameters. There are three main categories of morphing wings, namely in-plane alternation, out-of-plane transformation, and airfoil profile adjustment [15].

The in-plane alternation refers to the changes of wing shape that occurred in a two-dimensional (2D) plane (e.g. X- and Y-directions) wing plane, while the out-of-plane transformation refers to the changes of wing shape involved in Z-direction[17,18]. The in-plane morphing actuation is implemented through wingspan, sweep angle, and chord length changes, whereas the out-of-plane morphing is executed through the chordwise or spanwise bending and wing twisting actuation. The airfoil profile morphing is materialized through the application of wing camber and thickness adjustments[15].

The use of morphing wings along with low aspect ratio (LAR) wings (approximately AR = 1 to 1.5)[19] is the future design requirement of efficient MAV wings. However, the resulting LAR wings shall allow the flow vortices attached over most of the wing area, and therefore considerably affect its aerodynamic characteristics[20,21]. Previous studies have shown that these vortices are able to generate a nonlinear lift due to the low-pressure formation on the top wing surface, which consequently influences the induced drag components at high angles of attack[22)].

Induced drag plays a major contribution towards the over drag performances, which is highly associated with the wingtip vortices characteristics[23,24] Despite the empathize theory in the induced drag distribution, the influence of morphing wing mobility especially due to twist morphing wing deformation (wash in and wash out) towards the tip vortices characteristics and induced drag distribution on MAV wing size still remains unclear. Closest attempts of morphing MAV wing implementation can be found in the work of Ismail[25], who proposed a wash in twist morphing (TM) wings intending to improve the aerodynamic performances of MAV. The result showed that the wash in TM wings had a noticeably produced smoother lift behavior and capable of demonstrating a significant increase in lift performances[25,26]. However, the result also indicated that massive drag penalties were observed on the wash in TM wings, which also superior to the ones found on the rigid and membrane wings[25]. Thus, the main objective of this paper is to investigate the aerodynamic performances of another biomimetic morphing mobility known as wash out morphing wing. The investigation on the wash out morphing wing was executed with the purpose to improve the drag distribution of MAV wings and clarify the correlation between the wash out morphing wing vortices and their aerodynamic attributes. Technically, the wash out morphing wing has opposite deformation characteristics from the wash in morphing wing[18]. The force execution of the wash out morphing wing is identical to the wash in wing case study but with reverse vector direction. Table 1 summarizes the difference between the wash out and wash in twist morphing condition on the MAV wing. However, the current scope of works is not about to compare the aerodynamic performance between the wash in and wash out twist morphing wing. But it is executed to understand the correlation between the wash out morphing force variation towards its aerodynamics attributes. In this work, the Fluid-Structure-Interaction (FSI) simulation method was fully utilized, similar to previous works shown in reference[25]. The simulation was conducted using the quasi-static linear structural model in 3D combined with the fully utilized flow model in a steady state. The airflow domain was simulated through the FSI computational frameworks in the CFD commercial software. Three levels of the wash out morphing force (5N, 3N, and 1N) were used to evaluate the morphing performances together with the baseline wing models (membrane wing and rigid wing). Before the wash out morphing wing investigations were conducted, a verification of the FSI simulation method was executed by comparing simulation results with available experimental results.

2. Methodology

2.1 FSI Framework

The 3D, quasi-static, and linear structural models were used in this computational FSI framework to solve the deformation problems due to the morphing force. The FSI structural framework was then coupled with the steady-state, incompressible, and turbulent flow model, which solved based on Reynolds-averaged Navier Stokes (RANS) equations combined with SST turbulent model. The FSI framework (shown in Fig. 1) was fully implemented, which is similar to the previous morphing wing study found in the reference[25].

2.2 MAV Wing Model

Three levels of morphing force were implemented on a Zimmerman shape MAV wing known as TM 5N, TM 3N, and TM 1N (refer to Table 2) to elucidate the morphing conditions. The baseline wings (known as membrane wing and rigid wings) were also included in the comparison study. Each TM wing was modeled based on the previous works shown in reference[25]. In this work, the component of the fuselage (body), stabilizer (horizontal and vertical), and propeller were intentionally removed from the MAV models to avoid

any other aerodynamics influence (due to the components) on the TM wing results. The study focuses more on the wing aerodynamic performances rather than on the "ready-to-fly" MAV configuration. Thus, high attention is given on the wing's aerodynamic performances by excluding the fuselage, stabilizers, and propeller components. Based on previous studies[27,28], it shows that the fuselage and propeller attachment on MAV wing would require a complex system-level of design considerations and requirement. Contradiction in aerodynamic interest arises from multi-component MAV due to wing, fuselage, propeller and stabilizer aerodynamic design requirement. The aerodynamic influences presented by fuselage and propeller components shall dominate the flow behavior surrounding flow of MAV wing

Generally, all wings considered in this work have geometrical similarities in terms of shape, planform size, and overall wing dimensions with thickness maintained at 1 mm. However, the wings shape discrepancy was solely contributed by the morphing force magnitude (among the TM wing) and the membrane skin components (between the TM wings and baseline wings). The TM wings enforced with three levels of morphing force (5N, 3N, and 1N) with membrane skin components. Considering the MAV scale and its payloads size, the feasible morphing force magnitude generated on this wing must be relatively low. Hence, in this work, the maximum morphing force magnitude imposed on TM wing is limited at 5N, which is equivalent to the pull force provided by a 0.2 mm Flexinol® SMA wire[29]. Meanwhile, no morphing force was applied to the baseline wing configurations. The summary of wings similarities and discrepancies is given in Table 2. The coordinate system for each wing is set as follows: x is the chordwise direction, z is the spanwise direction, and y is the directed normal to the wing. The wing coordinate origin is set at the outer-most point of the wing leading edge.

Table 1. The deformation that distinguishes between wash out and wash in twist morphing on MAV wing.

	Non-morphing condition	**Wash in Twist Morphing**	**Wash out Twist Morphing**
Wing Deformation from Isometric view			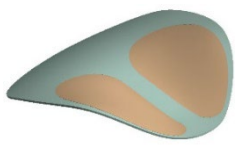
Wing Deformation from Side view			
Wing Deformation from Front view			

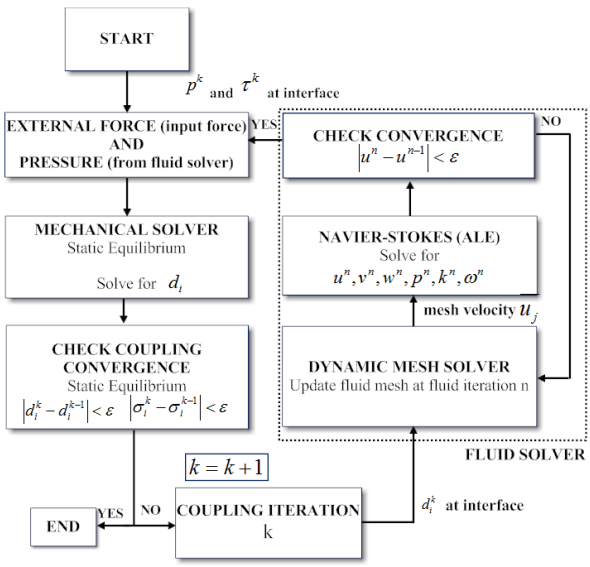

Fig. 1: FSI framework [25]

2.3 Mesh Characteristics and Material Properties for MAV Wing

The half wing geometry of TM wing and baseline wing (membrane and rigid) components are shown in Fig. 2. ABS plastic and silicone rubber material were assigned for the wing skeleton and membrane skin, respectively. The ABS plastic material selection was made based on the actual wing development that used 3D printing equipment and ABS plastic as its filament material. The material properties for the ABS plastic and silicone rubber material are listed in Table 3. For the simulation works, the wing skeleton and the membrane skin material were modeled as a linear elastic material. 3D hybrid mesh was used for the solid element for all wing components and models. The mesh independent study (for static structural analysis) was achieved with an optimized grid at 116,796 elements, as shown in Fig. 3.

Table 2. MAV wing characteristics.

	Wash Out TM 5N	**Wash Out TM 3N**	**Wash Out TM 1N**	**Membrane wing**	**Rigid wing**
Wingspan, b	150 mm	150 mm	150 mm	150 mm	150 mm
Root chord, c	150 mm	150 mm	150 mm	150 mm	150 mm
Aspect ratio, A	1.25	1.25	1.25	1.25	1.25
Morphing force component	F = 5 N	F = 3 N	F = 1 N	F= 0 N	F = 0 N
Membrane skin component	Included	Included	Included	Included	Excluded
Half wing geometry	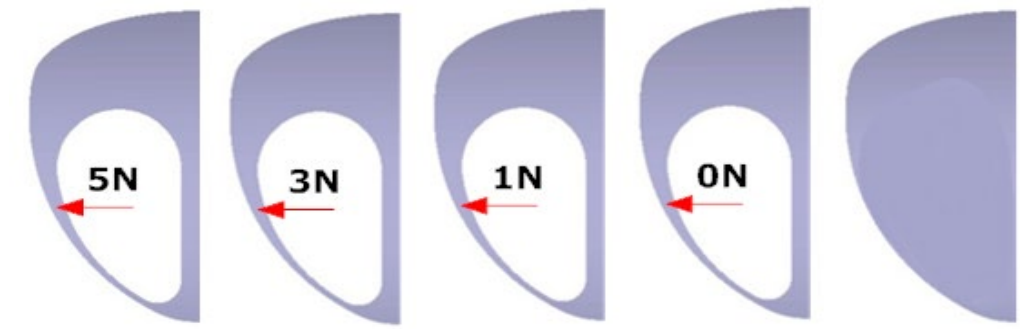				

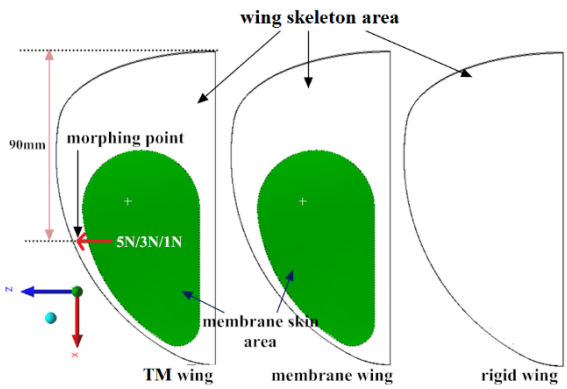

Fig. 2: TM wing component (half-wing view)

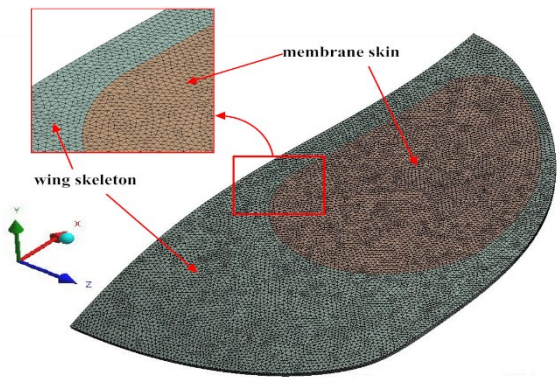

Fig. 3: The optimized mesh for solid component of wash out TM wing (half-wing view).

Table 3. The ABS Plastic material properties.

Physical Properties	**ABS Plastic**	**Silicone Rubber**
Density	1260 kg/m^3	1290 kg/m^3
Tensile Strength, Yield	43.4 MPa	2.5 MPa
Young's Modulus	2.27 MPa	6.5 MPa
Shear Modulus	0.8 GPa	2.2 GPa

2.4 The Static Structural Boundary Conditions of Morphing Wing

Fig. 4 shows the morphing principle behind the wash out TM wings concept. Due to the complexity and miniature size of morphing mechanism, the actual mechanism to induce the morphing mobility was not considered here as it was considered as beyond the current scope of works. Instead, only a virtual force was imposed on the TM wing to induce the morphing motion. In this work, the virtual force was imposed at a 45° angle, as shown in Fig. 4, directed upwards with the objective to produce a local wing deformation, especially near the wingtip. the centerline (root) of the wing is imposed as the fixed end to replicate the similar experimental setup as shown in reference[30]. Three levels of morphing force magnitude (1 N, 3 N, and 5 N) pointed near the wingtip to ensure the

morphing condition achieved. The point location is an optimized morphing point, as determined by the previous morphing study shown in the reference[30]. As expected, the morphing point located at the wingtip effectively produced a significant wing deformation, as shown in Fig. 5, which resulted in a wash out morphing condition on each TM wing. The wash out morphing level found on each TM wing was clarified based on its magnitude of geometric twist (ϵ), which was obtained from the local angle of attack extraction method shown in reference[31]. The wing deformations results with its ϵ magnitude are given in Fig. 5. Theoretically, the deformation found on the baseline and TM wings is mainly contributed by two main sources; the aerodynamic loads and the morphing forces[6]. The results exhibited that there was no significant wing deformation found on the baseline wings. It means that the aerodynamic loads which were solely enforced on the baseline wing surface were not intense enough to deform the wing. Thus, the baseline wings maintained their original ϵ magnitude at ϵ = 0.5°. Instead, the virtual morphing force which was found on TM wing produced a wash out wing deformation on every TM wing significantly. The level of wash out twist morphing characteristics was denoted through its negative ϵ magnitude[31]. As expected, the TM 5N wing produced the largest wash out twist morphing characteristic among the wing with ϵ magnitude at ϵ = -12.7°. This was followed by the TM 3N and TM 1N wings at ϵ = -8.5° and -3.0°, respectively. Based on these ϵ results, it can be concluded that aerodynamic loads have a minimum impact on the overall wing deformation and ϵ magnitude compared to the morphing forces. Instead, the morphing force showed a substantial influence on the overall wing deformations and ϵ magnitude. In fact, TM wings with higher morphing force exhibited greater wing deformations, which consequently induced a higher level of wash out twist morphing characteristics based on the negative ϵ magnitude.

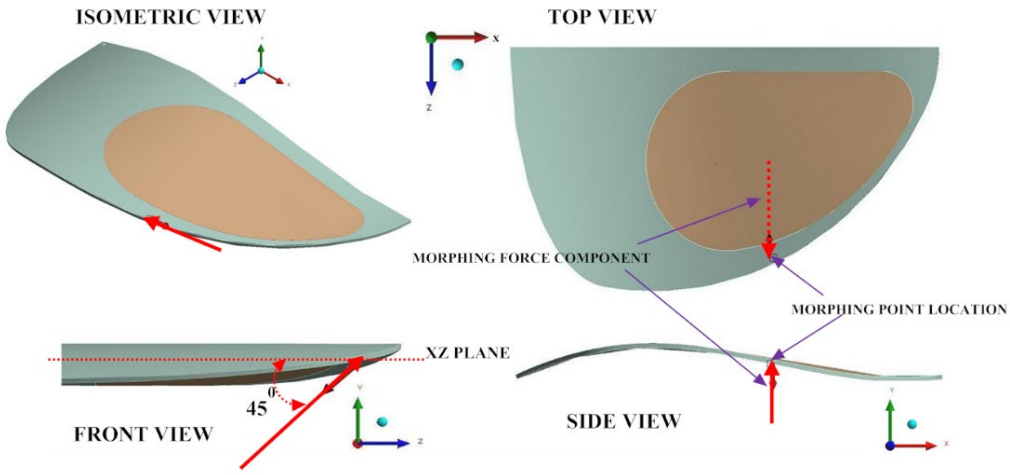

Fig. 4: The imposed morphing force on wash out TM wing (half-wing view)

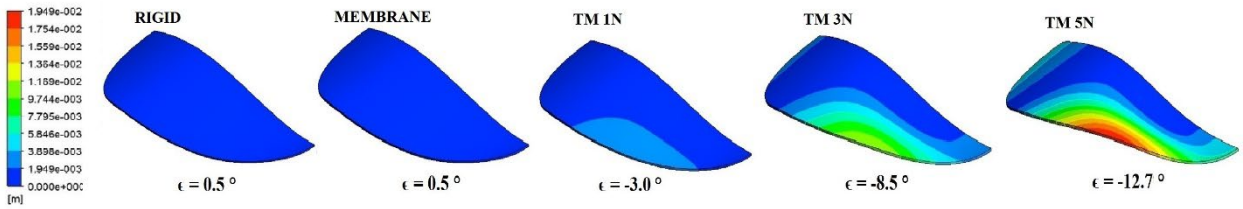

Fig. 5: The wing deformation and geometric twist (ϵ) for all wing (half-wing view).

2.5 The Flow Field Boundary Conditions Surrounding Morphing Wing

In this work, the symmetrical geometrical condition was fully implemented for the 3D computational flow domain surrounding the wash out TM wing. The size of the 3D domain size was built relative to the root chord unit (c), as shown in Fig. 6. The mesh independent studies were carried out (as shown in Table 4) to evaluate the quality of the constructed numerical mesh grid. Based on the mesh independent study, the optimized grid was achieved at 661,247 elements (case 3), as shown in Fig. 7. Mesh with y+ ≤ 1 criteria achieved to ensure the boundary layers phenomenon on the wing surfaces were sufficiently captured. The inlet and outlet boundary conditions applied at the 3D flow domain and marked by flow vectors shown in Fig. 6. The inlet flow velocity is set to maintain at 9.5 m/s (equivalent to Re = 100,000 at the root chord) which is the common speed for MAV wing operation. For the airflow simulation continuity, a zero-pressure boundary condition is implemented at the outlet. The wall on the

wing-half side is defined as a symmetrical wall, while the opposite wall is defined as a slip surface condition. The wing surface itself is defined as a no-slip boundary and surface boundary for FSI interaction. For the aerodynamics variation study, the wing angle of attack (α) was defined at the wing root and set to be increased from -10° to 35° with 2° interval. The ideal air properties assign for the flow domain, which is given in Table 5. In the current work, the convergence criteria for the wing static structural and fluid simulation solver are set based on the root mean squared error value with the magnitude of 10^{-5} to ensure the solution accuracy.

Table 4 The mesh independent studies executed at α = 10 °, Re = 100,000, Wash Out TM 5N wing

	Case 1	Case 2	Case 3	Case 4	Case 5
Total elements	167, 521	335, 541	661, 247	1,221, 516	2,402, 533
CL	0.123	0.098	0.246	0.244	0.244
CD	0.039	0.051	0.0643	0.063	0.064
CM	-0.034	-0.040	-0.114	-0.112	-0.113

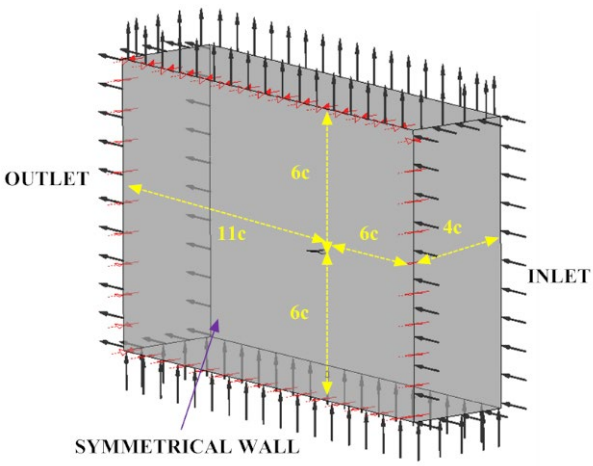

Fig. 6: The computational domain size

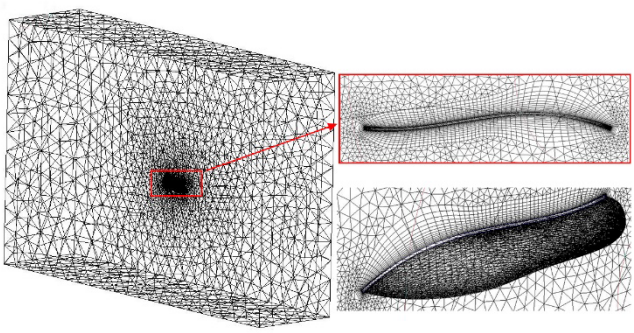

Fig. 7: The optimized grid for wash out TM wing

Table 5 The Ideal Air Properties at 25 °C

Properties	Value
Density	1.185 kg/m3
Dynamic Viscosity	1.831×10^{-5} Pa
Reference Pressure	1 atm

3. Results and Analysis

3.1 Verification on FSI Simulation Method

Verification on the FSI simulation method was conducted to justify the method in predicting the twist morphing wing performances. The experimental data from previous works[30)] were adopted and compared with predicted data produced by the current FSI simulation method. The verification works concentrated on two main aerodynamic parameters known as the lift coefficients (C_L) and drag coefficient (C_D) results. Fig. 8 shows the lift coefficient (C_L) and drag coefficient (C_D) results for 5N force wash in twist morphing MAV wing with a speed of 9.5 m/s (Re≈100,000 at chord). The results show that the C_L and C_D results (simulation curves) predicted by the FSI simulation method remained close to the experimental data (experimental dots) starting from low α (α = -10°) magnitude up to high stall angle (α ≈15°). The results clearly show that the simulation satisfactorily captured the significant trend found in overall C_L and C_D results with a slight discrepancy in magnitude (below 10%) compared to the experimental results. However, as the α increased beyond the stall angle, the simulation curve began to deviate at a lower magnitude compared to the experimental results. Such characteristic typically happens as the RANS SST k-ω turbulent model insufficiently captures high turbulent phenomenon and organized transient motion produced at the post-stall angle[25,30)]. Despite this discrepancy, the general trend of the C_L and C_D magnitude and their increment with α value were satisfactorily predicted by the FSI simulation. A strong correlation between the simulation and experimental results is clearly shown, particularly at the α region below the stall angle (pre-stall angle). Thus, it can be concluded that the FSI simulation method applied in this work is satisfactorily verified to be employed in further morphing investigations.

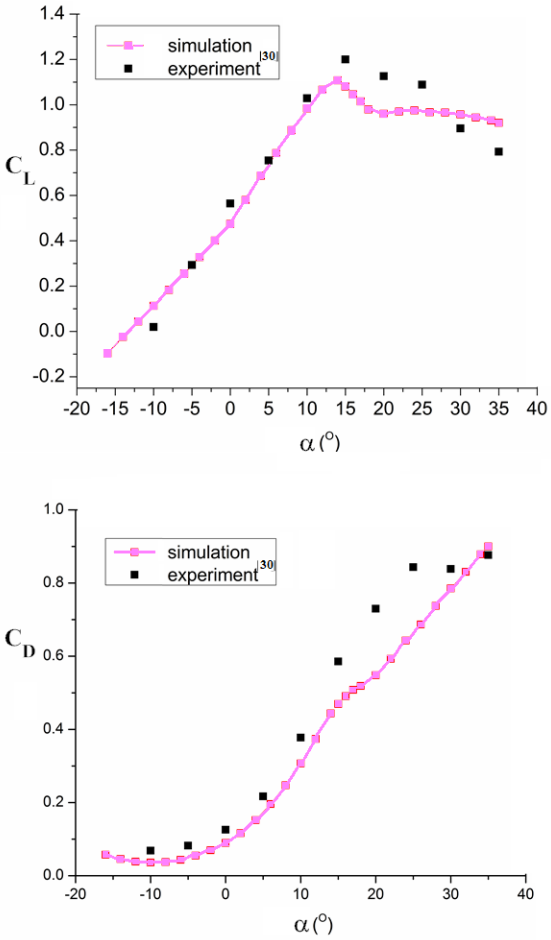

Fig. 8: Comparison of C_L (top) and C_D (bottom) performance based on simulation and experimental results[30] on wash in 5 N twist morphing wing at 9.5 m/s.

3.2 Lift Coefficient

Fig. 9 Lift coefficients (C_L) results for the wash out TM wings (TM 1N, TM 3N, TM 5N), and the baseline wings (rigid, membrane) throughout the α region are given in Fig. 9. In general, the trend of lift curves for all wings was commonly seen where the magnitude of C_L increases with α increment. A clear linear increment trend for all wing is found in the C_L slope started at α = 0° until the stall condition (α_{stall}).

These results show that the wash out TM wings demonstrate a substantial C_L decrease in the lift curve (between 5% and 23%) from TM 1N to TM 5N wing. Based on these results, the wash out TM 5N wing produces the lowest maximum lift coefficient (C_{Lmax}) at C_{Lmax} = 0.92. This is followed by the wash out TM 3N (C_{Lmax} = 1.0) and TM 1N (C_{Lmax} = 1.08) wings compared to the rigid (C_{Lmax} =1.20) and membrane wings (C_{Lmax} = 1.13).

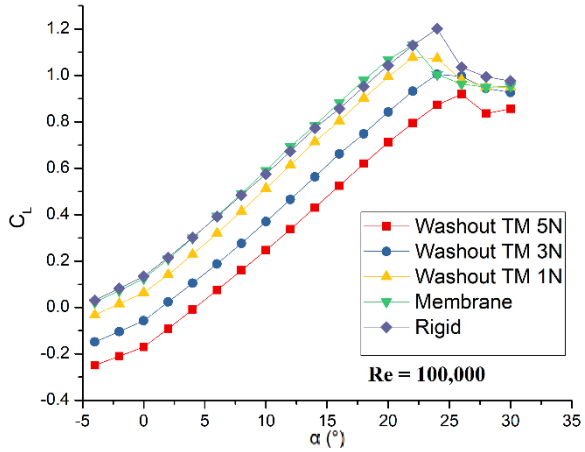

Fig. 9: Lift coefficient performances for all wings.

Analysis of α cases between α = 0° and 22°clearly shows that all wash out TM wings produced lower C_L magnitude compared to the baseline wings. On average, wash out TM 1N and TM 3N wings produced between 4% and 50% lower C_L magnitude than the baseline wings. In fact, TM 5N significantly produced two times lower C_L magnitude than the baseline wings. Based on this attribute, it highlights the drawbacks of wash out morphing motion on the overall C_L distribution of wash out TM wing. The wash out TM wings have lowered the C_L distribution than the baseline wings. In fact, the wash out TM wing with higher morphing force has lower C_L distribution.

Based on stall angle (α_{stall}) characteristics, the rigid and wash out TM 3N wings surprisingly induced similar α_{stall} magnitude at α_{stall} = 24°, while the membrane wing showed identical stall angle to the wash out TM 1N wing at α_{stall} = 22°. However, the wash out TM 5N wing produced a more delay stall angle at α_{stall} = 26° in which, the highest stall angle among the wings. This exhibits that wash out TM 5N wing is able to induce at least 8.3% better α_{stall} angle compared to the baseline wing. Despite better α_{stall} performances exhibited by almost all wash out TM wings, the results needed to be carefully considered due to turbulent model capability in predicting the α_{stall} performance, which was near the stall region.

In terms of zero-lift angle of attack ($\alpha_{CL=0}$) characteristics, all wash out TM wings exhibited higher $\alpha_{CL=0}$ magnitude compared to rigid and membrane wings. TM 5N wing induced the highest $\alpha_{CL=0}$ magnitude at $\alpha_{CL=0}$ = 4.3°. While TM 3N induced $\alpha_{CL=0}$ magnitude at $\alpha_{CL=0}$ = 1.4° and the TM 1N wing exhibited a $\alpha_{CL=0}$ negative value ($\alpha_{CL=0}$ = -2.7°). The rigid and membrane wings also exhibited a negative value of $\alpha_{CL=0}$ at -5.2° and -4.9°, respectively.

Detailed analysis of C_L increment magnitude ($C_{Lincrement}$) was also conducted at the incline angle (α= 5° to 10°). The analysis shows that the wash out TM 5N and TM 3N wings induced the lowest $C_{Lincrement}$ magnitude at 70% and 75%, respectively. Wash out TM 1N wing induced the highest $C_{Lincrement}$ among the morphing wing

at $C_{Lincrement}$ = 84%. However, the baseline wings (rigid and membrane) induced better C_L magnitude increment at $C_{Lincrement}$ = 90% and 97%, respectively.

Based on the overall C_L performances, a significant effect of wash out twist morphing is established. Wash out morphing motion on TM wings clearly induced a few drawbacks in its overall C_L performances by degrading the C_L magnitude, C_{Lmax}, $\alpha_{CL=0}$, and $C_{Lincrement}$ performances. In fact, TM wings with higher morphing force showed inferior overall C_L performances.

3.3 Drag Coefficients

The drag coefficient (C_D) results for all wings throughout the α region are shown in Fig. 10. In general, every wing performs a gradual decrease in drag magnitude at early α region (-4° < α < 6°), before it reaches the minimum drag magnitude known as the C_{Dmin} point. After the C_{Dmin} point, every wing performs a dramatic increase in C_D magnitude approaching the stall region (α_{stall} = 22°-26°). Every wing showed a slight halt in the C_D increment, particularly at the early post-stall angle (1° to 2° after stall). But the halt was recorded below than a 2% drop of C_D magnitude before it continued to increase monotonically at least 12 % at higher post-stall wing incidence. The C_D magnitude kept on increasing after the stall angle.

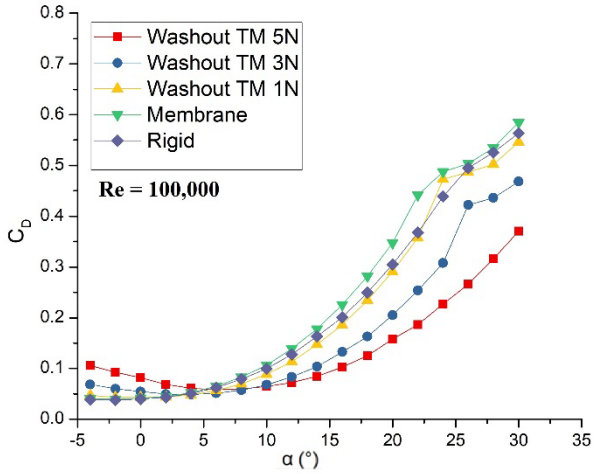

Fig. 10: Drag coefficient performances for all wings

Based on the overall trend, the C_D curve for the baseline, wash out TM 1N, and TM 3N wings performed almost similarly before the C_{Dmin} point (C_{Dmin}= 0.04 at α= -2°). After the C_{Dmin} point, the results show that the membrane wing drastically deviated at a greater C_D magnitude, which left the other wing at a lower C_D level. The rigid wing induced a slightly lower C_D level than the membrane wing but marginally higher than the wash out TM 1N wing. However, wash out TM 3N and TM 5N wings had a significantly lower C_D trend compared to the other wings. Initially, such C_D trends highlighted the influence of the wash out morphing wing in reducing the C_D magnitude at α region after C_{Dmin} point. Further analysis was conducted to compare the C_D performances among the wings.

Detailed analysis of C_{Dmin} magnitude exhibited that, in general, the baseline wings had a lower magnitude of C_{Dmin} than all wash out TM wings. It was recorded that the C_{Dmin} point for the baseline wings occurred at a lower α compared to the wash out TM wings. Wash out TM 5N wing had the highest C_{Dmin} = 0.06, which occurred at α= 6°. This is followed by the wash out TM 3N (at C_{Dmin}= 0.05 at α= 4°) and TM 1N (C_{Dmin} = 0.04 at α= 0°) wings. The rigid and the membrane wings had identical and the lowest C_{Dmin} magnitude among the wings at C_{Dmin} = 0.03 and α= -2°. However, as the α increased beyond the C_{Dmin} point, TM wings considerably lowered C_D magnitude compared to the baseline wings. Detailed analysis at a pre-stall angle (α= 5° to 25°) shows that wash out TM 5N wing averagely produced 71% lesser C_D magnitude than the membrane wing. This was followed by wash out TM 3N and TM 1N wing, which averagely induced about 49% to 15% better C_D magnitude than the membrane wing. Such a result indicated that the wash out TM wings induced significantly lower C_D magnitude than the baseline wings, particularly at α between 5° and 25°.

Analysis of such benevolent C_D performance can be further clarified through the C_D increment rate ($C_{Dincrement}$) analysis, which averagely taken at every 2° of α increment. The analysis was also specifically conducted at α cases beyond the C_{Dmin} point (α= 5° to 25°). The result has revealed that as the α increase beyond α = 5°, there was a remarkable increase in C_D magnitude, especially for the baseline wings. The baseline wings induced the highest C_D increment rate at $C_{Dincrement}$= 22% for every 2° of α increment. This was followed by wash out TM 1N and TM 3N wings at $C_{Dincrement}$= 20% and 16%, respectively. Wash out TM 5N wing remarkably induced the lowest C_D increment rate among the wings at $C_{Dincrement}$= 12%. Based on these $C_{Dincrement}$ and C_D magnitude analyses, the results imply that wash out TM wings promisingly induced lower drag penalty compared to the baseline wings, notably at α cases between 5° and 25°. Thus, higher morphing force on wash out TM wings induced better C_D performance, which may offer a good advantage for MAV in improving its cruise-speed condition and power-saving flight.

3.4 Moment Coefficients

The longitudinal pitching moment (C_M) result, which took at the wing leading edge, is presented in Fig. 11. The C_M result is given in the lift coefficient (C_L) function for C_M curve slope ($\Delta C_M/\Delta C_L$) analysis, which was used to indicate the level of the nose-down moment and further represented as initial evaluation on the MAV longitudinal static stability performance. Steeper C_M curve slope indicate larger static margins: stability concerns are a primary target of design improvement from one generation of micro-air vehicles to the next. The range of flyable CG locations is generally only a few millimeters long; meeting this requirement represents a strenuous weight management challenge on MAV[6]. In general, it is found that the C_M slope has a strong function of α with

negative C_M slope recorded for all wings. This condition indicates that each wing is able to produce a nose-down moment that is essentially required for MAV longitudinal static stability. Detailed $\Delta C_M/\Delta C_L$ analysis was further conducted at the linear C_M curve region between C_L= 0.0 and 0.6.

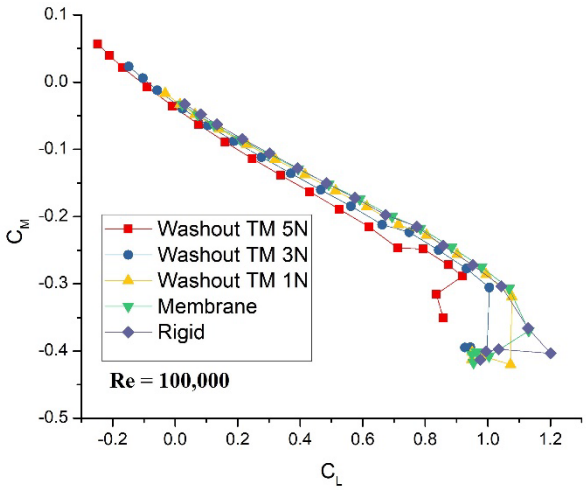

Fig. 11: Moment coefficient performances for all wings

The $\Delta C_M/\Delta C_L$ analysis result shows that wash out TM 5N wing produced the steepest C_M slope with $\Delta C_M/\Delta C_L$= -0.31. This is followed by wash out TM 3N and TM 1N wings at $\Delta C_M/\Delta C_L$= -0.28 and $\Delta C_M/\Delta C_L$= -0.27, respectively. Meanwhile, the baseline (rigid and membrane) wings have a slightly higher $\Delta C_M/\Delta C_L$ magnitude than the wash out TM wings at $\Delta C_M/\Delta C_L$= -0.25. Based on these results, it was found that wash out TM wings showed a slight advantage by producing better longitudinal static stability due to steeper C_M curve slope results. A wash out TM wing produced at least 8% more negative $\Delta C_M/\Delta C_L$ magnitude than the baseline wings. However, the current $\Delta C_M/\Delta C_L$ result only presented as an initial stability finding, which warrants further investigation that is way beyond the interest of the current study.

3.5 Aerodynamics Coefficients

Based on the C_L and C_D results mentioned above, the aerodynamic efficiency (C_L/C_D) performance for each wing is presented in Fig. 12. Aerodynamic efficiency is a derive function through the ratio between C_L and C_D at a given α case. Overall, the results show that each wing produces an almost similar trend of C_L/C_D curve. The C_L/C_D curve starts at low C_L/C_D value at α below 0° before the C_L/C_D magnitude increases up to its maximum point (known as maximum C_L to C_D ratio point or $C_L/C_{D\,max}$) at α between 6° to 16°. After the $C_L/C_{D\,max}$ point, the C_L/C_D curve starts to decrease monotonically at lower C_L/C_D value until the stall condition produced at α between α_{stall} =24° to 26°.

The $C_L/C_{D\,max}$ results clearly show that the rigid wing had the highest $C_L/C_{D\,max}$ magnitude with $C_L/C_{D\,max}$= 6.32, which also constituted as the best aerodynamic efficiency among the wings. This was closely followed by the membrane wing with $C_L/C_{D\,max}$ = 6.08. Based on the detailed analysis of $C_L/C_{D\,max}$ magnitude, the result shows that the baseline had at least 2% better $C_L/C_{D\,max}$ magnitude than the wash out TM wings. Wash out TM 1N wing only managed to produce the best aerodynamic efficiency among the wash out TM wing with $C_L/C_{D\,max}$ = 5.97. It was closely followed by the wash out TM 3N at $C_L/C_{D\,max}$= 5.59. However, wash out TM 5N had the least $C_L/C_{D\,max}$ magnitude among the wing with $C_L/C_{D\,max}$= 5.12.

Based on the $C_L/C_{D\,max}$ occurrence point, the baseline wings were found to occur coincidentally at α = 6°, while the wash out TM wings were seen to produce the $C_L/C_{D\,max}$ at a relatively higher inclined angle between α = 8° to 16°). The occurrence of the $C_L/C_{D\,max}$ at higher α (compared to baseline wings) was interestingly analogous to its intrinsic advantage in extending the $\alpha_{stall,}$ as shown in Fig. 9.

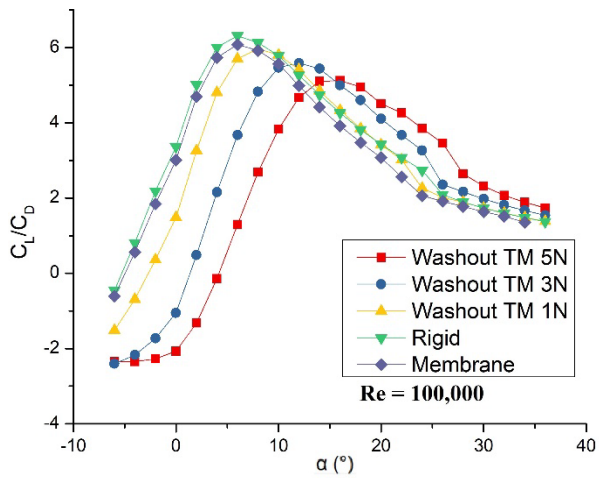

Fig. 12: Aerodynamic efficiency performances for all wings.

As a conclusion to this performance, it clearly shows that the trade-off between degrading C_L performance (low C_L magnitude, C_{Lmax}, $\alpha_{CL=0,}$ and $C_{Lincrement.}$) while improving C_D performance (low $C_{Dincrement}$ and C_D magnitude) seemed to affect the aerodynamics efficiency of all wash out TM wings. The aerodynamics efficiency trade-offs were vastly visible for all wash out TM wings, in which the wing had at least 2% aerodynamically less efficient than the baseline wings. Apparently, the benevolent C_D performances found on the wash out TM wings were significantly overwhelmed by the malevolent C_L performances. The advantages found in the C_D performances still could not overcome the drawbacks of C_L performances. Further investigations on the vortex formation and pressure distribution over the baseline and wash out TM wing surfaces were carried out to explain the reason behind the drawbacks in C_L and the advantages of C_D performances.

3.5 Vortex Formation and Pressure Distribution on Wash Out TM Wing Surface

The investigation of vortex formation and pressure distribution over the baseline and wash out TM wing surfaces is very useful to explain the reason behind the degradation of C_L and the improvement of C_D performances. Thus, this current study on vortices was established based on the method used by Ismail[22)], as shown in Fig. 13. The method used the approximation type measurement to estimate the maximum diameter and length of tip vortices (TV) and leading-edge vortices-tip vortices (LEV-TV) interaction based on wing chord length (c). TV is clearly produced downstream of the wingtip. While the LEV-TV is located at the wingtip which is the edge of LEV and at the beginning of TV. The visualization of these vortices formations was highlighted (noted as blue color contour) using limited Q criterion magnitude with ISO-contours of Q = 3.0. The vortices observation was viewed only at the half wing due to the symmetrical existence of vortices and wing conditions. The vortices measurements were designated as follows; TV diameter (DTV), TV length (LTV), and LEV-TV diameter (DLEV-TV). The sizes of DTV, LTV, and DLEV-TV were used to indicate the strength of the vortex's formations. Larger DTV, LTV, and DLEV-TV sizes indicated stronger vortices and vice versa. The sizes of DTV, LTV, and DLEV-TV were also used to correlate with the C_L and C_D performances found on the baseline and wash out TM wings.

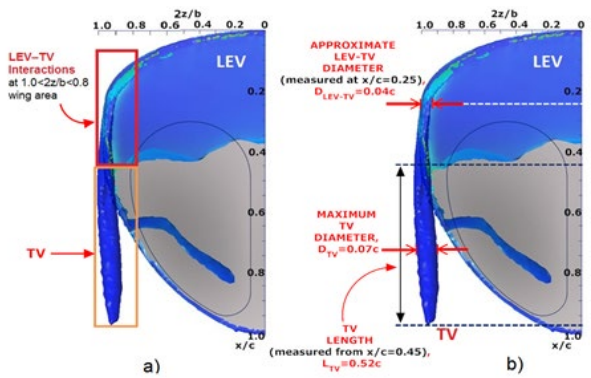

Fig. 13: a) LEV-TV Interaction Area b) The Location and Measurement of DTV, LTV and DLEV-TV [22)]

Fig. 14 shows the vortices formation (noted by blue contour) generated on the wash out TM and baseline wings at α= 14°. The 14° angle was chosen since the wing incidence fell within the linear C_L curve region and away from any stall occurrence. In general, the results apparently show that all wings produced a distinct generation of the TV and LEV–TV interactions structure. The most noticeable TV and LEV-TV structures were found on the membrane and rigid wings. The baseline wings were noted to have produced DTV = 0.09c ~ 0.10c and LTV = 0.54c ~ 0.055c. Wash out TM 1N wing also induced a visible TV and LEV-TV structures with DTV = 0.06c and LTV = 0.38c. These DTV and LTV magnitudes were at least 50% (for DTV) and 42% (for LTV) smaller than the baseline wings produced. The vortices deficiency trend continued for wash out TM 3N and TM 5N wings, where both wings produced at least two times smaller DTV and LTV magnitudes compared to the baseline wings. Based on this result, it can be explained that DTV and LTV deficiency trend has a good correlation with the C_D performance on the wings. Apparently, the high magnitude of C_D (shown in Fig. 10) induced by the baseline wings (C_D= 0.163 ~ 0.177) highly constituted by its large DTV's and LTV's sizes (DTV = 0.09c ~ 0.1c and LTV = 0.54c ~ 0.055c). Meanwhile, smaller DTV's and LTV's sizes produced on the wash out TM wings (DTV = 0.06c ~ 0.4c and LTV = 0.38c ~ 0.3c) induced lower C_D magnitude (C_D = 0.147 to 0.084).

The analysis of DLEV-TV formations also showed that there was a significant DLEV-TV deficiency induced by the wings. Obviously, the baseline wings had larger DLEV-TV (DLEV-TV= 0.08c~ 0.11c) compared to the wash out TM wings (with DLEV-TV= 0.02c~ 0.07c). According to Ismail[7)], the DLEV-TV formation contributes to the intensity of low-pressure cells in the same area of LEV-TV interactions (shown in Fig. 13). The evidence of low-pressure cells induces found on each wing surfaces is presented in Fig. 15. The results on the lowest pressure coefficient (denoted as C_{pmin}) magnitude induced at the LEV-TV interactions area are particularly highlighted to elucidate the low-pressure cells (denoted by mostly blue color contour). C_{pmin} magnitude was used in the analysis to correlate with the level of the LEV-TV interactions and further verify the C_L performance found on each wing. Based on the result of low-pressure cells (Fig. 15), it was found that the baseline wings induced the lowest C_{pmin} magnitude at C_{pmin}= -2.01 to -2.11. Such C_{pmin} performances constituted by their large DLEV-TV size (DLEV-TV= 0.08c~ 0.11c), which was also associated with their strong LEV-TV interactions. These conditions provided the evidence behind the superior C_L performance (C_L= 0.784~0.773) found on the baseline wings, as shown in Fig. 9. Wash out TM wings show consistent evidence where the higher magnitude of C_{pmin} was induced by smaller DLEV-TV size, which also means weaker LEV-TV interactions compared to the baseline wings produced. wash out TM 1N and TM 3N produced C_{pmin}= -1.79 and -1.23, respectively. Meanwhile, wash out TM 5N wing induced the highest C_{pmin} magnitude at C_{pmin}= -0.69. Such C_{pmin} performances constituted by their smaller DLEV-TV size (DLEV-TV= 0.07c~ 0.02c), which also means weaker LEV-TV interactions. These conditions are considered significant evidence behind inferior C_L performance found on the wash out TM wings, which were recorded at C_L= 0.430~0.714.

Based on these results, it can be concluded that the wash out TM wings showed better C_D performances compared to the baseline wings. The morphing force on wash out TM wing significantly deformed the wing and promoted

smaller and weaker DTV and LTV structures than the baseline wing. Such conducive DTV and LTV structures led to better C_D performances for wash out TM wings. In fact, wash out TM wings configuration with higher morphing force had better C_D performances due to more favorable DTV and LTV structures. Such C_D performances were seen as the evidence in improving the drag distribution over the MAV wings.

However, wash out TM wings also endured huge drawbacks by producing inferior C_L performances. The morphing wing deformation consequently induced smaller DLEV-TV size and weaker LEV-TV interactions compared to the baseline wings. The weak LEV-TV interactions subsequently contributed to a substantially adverse pressure on the wash out TM wings, which led to its inferior C_L performance.

Resulting from the thread-off between the C_L and C_D performances, the magnitude of C_L/C_D for the wash out TM wings was well affected. The aerodynamic efficiency of wash out TM wings was obviously overwhelmed by the degradation of C_L performances which could not be recovered through the drag improvement. As a result, wash out TM wings suffered from less aerodynamics efficiency compared to the baseline wings. The degradation of C_L and C_L/C_D found on wash out TM wings was seen as the malevolent performance on such high potential of a biomimetic morphing wing.

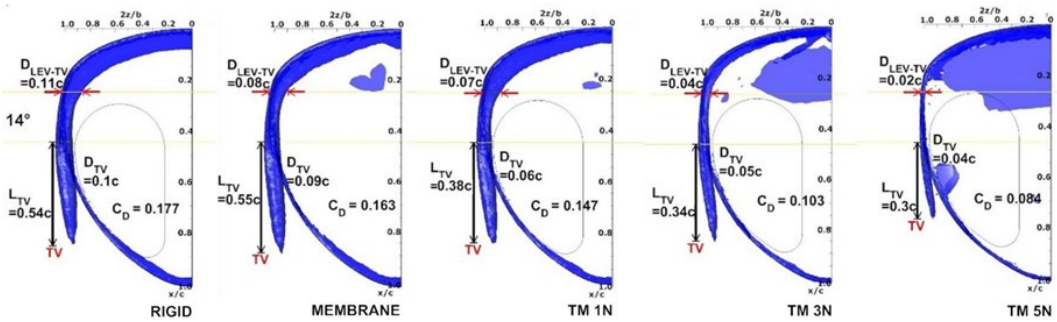

Fig. 14: Vortex formations over the wash out TM and baseline wings.

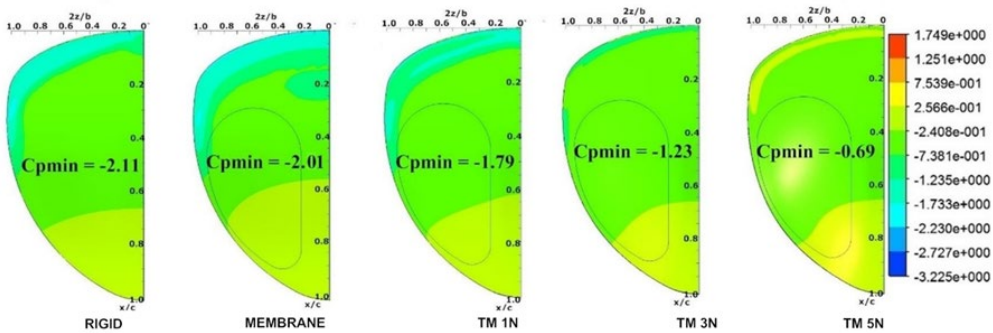

Fig. 15: Pressure Distribution and Magnitude of C_{pmin} over the wash out TM and baseline wings (half wing view) at α=14°.

4. Conclusion

In this work, an FSI simulation was used to investigate the wing aerodynamics for wash out TM wings. The aerodynamic performance of wash out TM wings was compared with the rigid and membrane wing with the intention to elucidate the lift, drag and aerodynamic efficiency of the wings. The simulation works were executed based on steady state, incompressible flow, coupling of quasi-static aeroelastic structural analysis and RANS-SST turbulent solver model.

The FSI simulation method was initially verified by comparing the simulation results with available experimental data on wash in TM wings. The verification results showed that the FSI simulation model had satisfactorily captured the significant trend and magnitudes found in overall C_L and C_D results, especially at the α region below the stall angle.

Based on the wing structural deformation results, it was evident that the aerodynamic loads, solely enforced on the baseline wing surface, are not intense enough to deform the wing or alter its ϵ magnitude. Instead, the virtual morphing force, which was found on wash out TM wings, significantly induced a wash out wing deformation. In fact, wash out TM wings with higher morphing force induced larger wing deformation and resulted in a more significant negative ϵ magnitude. As expected, wash out TM 5N wing was found as having the largest wing deformation and negative ϵ magnitude among the wings. In contrast, the baseline wings exhibited very minimum deformations and only remained at its original ϵ magnitude.

C_L results exhibited that the wash out TM wings have lesser C_L magnitude, which is about 4% or two times lower than the baseline wings produced. As a result, the wash out TM wings have produced inferior C_L, C_{Lmax}, $\alpha_{CL=0}$ magnitudes and $C_{Lincrement}$ performances compared to

the baseline wings. Furthermore, wash out TM wings, which carry higher morphing force, have induced poorer C_L performances. The vortex formation and pressure distribution investigations have revealed that such C_L degradation found the wash out TM wing is due to weak LEV-TV interactions, which lead to substantial adverse pressure on the wash out TM wings.

On the other hand, the wash out TM wings have shown better C_D performances compared to the baseline wings in terms of C_D and $C_{Dincrement}$ magnitude especially at α cases between 5° and 25°. wash out TM wings managed to produce at least 15% better C_D magnitude than the membrane wings. In fact, wash out TM wings which carry higher morphing force have induced better C_D and $C_{Dincrement}$ performances. Such conditions imply that wash out TM wings have promisingly induced lower drag penalty compared to the baseline wings. The investigation on the vortices formation discovered that the wash out TM wings have weaker DTV and LTV formations than the baseline wings which have subsequently induced lower C_D and $C_{Dincrement}$ magnitude on the morphing wings. Such C_D performance is seen as main benevolent performance for the morphing wings.

Due to the trade-off between C_L and C_D performance, the aerodynamics efficiency of all wash out TM wings has been well affected. The magnitude of aerodynamics efficiency for all wash out TM wings is at least 2% less efficient than the baseline wings. Obviously, the C_D advantages found on the wash out TM wings are still unable to overcome the drawbacks of C_L performances which in turn, reducing its overall aerodynamics efficiency performances.

The investigation of vortices formation and pressure distribution supports the C_L and C_D findings on wash out TM wing by showing that the wings have a conducive vortices formation but with adverse pressure gradient. wash out TM wings are able to promote smaller and weaker DTV and LTV structures which lead to better C_D performances. However, the wings also endure drawbacks by inducing smaller DLEV-TV size and weaker LEV-TV interactions. Such conditions have substantially induced adverse pressure on the wing surfaces and lower its C_L performances.

Therefore, future works should be conducted on the experimental validation of the aerodynamics, vortices formation and aeroelastic characteristics on wash out TM wing.

Acknowledgements

Authors acknowledge technical and financial support from Universiti Teknologi MARA Cawangan Pulau Pinang and the Government of Malaysia.

Nomenclature

μ	Micro
C_L	Lift coefficient
C_D	Drag coefficient
C_{Lmax}	Maximum lift coefficient
C_{Dmin}	Minimum drag coefficient
L	Total chordwise length
y+	y value of first cell
α	angle of attack
$\alpha_{CL=0}$	zero-lift angle of attack
α_{stall}	stall angle
DTV	TV diameter
LTV	TV length
DLEV-TV	LEV-TV diameter

References

1) Shuvrangshu Jana, Harikumar Kandath, Mayur Shewale, Gunjit Dhingra, Duddela Sai Harish, and M. Seetharama Bhat, "Design and development of a novel fixed-wing biplane micro air vehicle with enhanced static stability," *CEAS Aeronautical Journal*, **13** 433–452 (2022). doi:https://doi.org/10.1007/s13272-022-00570-w.
2) J.M. Grasmeyer, and M.T. Keennon, "Development of the Black Widow Micro Air Vehicle," in: 39th AIAA Aerospace Sciences Meeting and Exhibition, Simi Valley, CA, 2001: pp. 1–9.
3) N.I. Ismail, H. Sharudin, M.M. Mahadzir, Z.M. Ali, A.A. Shariffuddin, and N.I. Kamel, "Computational aerodynamics study on neo-ptero micro unmanned aerial vehicle," *Evergreen*, **8** (*2*) 438–444 (2021). doi:10.5109/4480726.
4) T. Nakata, H. Liu, Y. Tanaka, N. Nishihashi, X. Wang, and A. Sato, "Aerodynamics of a bio-inspired flexible flapping-wing micro air vehicle," *Bioinspiration & Biomimetics*, **6** (*4*) 1–11 (2011). doi:10.1088/1748-3182/6/4/045002.
5) T.N. Dief, and S. Yoshida, "System identification for quad-rotor parameters using neural network," *Evergreen*, **3** (*1*) 6–11 (2016). doi:10.5109/1657380.
6) B.K. Stanford, P. Ifju, R. Albertani, and W. Shyy, "Fixed membrane wings for micro air vehicles: experimental characterization, numerical modeling, and tailoring," *Progress in Aerospace Sciences*, **44** (*4*) 258–294 (2008). doi:10.1016/j.paerosci.2008.03.001.
7) N.I. Ismail, "Aerodynamic Performances and Flow Structure Investigations On Active Twist Morphing MAV Wing," Universiti Teknologi MARA, 2014.
8) D.D.D.P. Tjahjana, I. Yaningsih, B.Y.L. Imama, and A.R. Prabowo, "Aerodynamic performance enhancement of wing body micro uav employing blended winglet configuration," *Evergreen*, **8** (*4*) 799–811 (2021). doi:10.5109/4742122.

9) M.R. Ahmed, and M.M. Abdelrahman, "Optimal wing twist distribution for roll control of mavs," *The Aeronautical Journal*, **115** (*1172 641*) 641–649 (2011).
10) W. Shyy, "Membrane wing-based micro air," *Applied Mechanics Reviews*, **58** (*July*) 283–301 (2005). doi:10.1115/1.1946067.
11) T.N. Dief, and S. Yoshida, "System identification and adaptive control of mass-varying quad-rotor," *Evergreen*, **4** (*1*) 58–66 (2017). doi:10.5109/1808454.
12) J.T. Cantrell, B.W. LaCroix, and P.G. Ifju, "Passive roll compensation on micro air vehicles with perimeter reinforced membrane wings," *51st AIAA Aerospace Sciences Meeting*, **5** (*3*) 1–12 (2013). doi:10.1260/1756-8293.5.3.163.
13) B. Stanford, M. Abdulrahim, R. Lind, and P. Ifju, "Investigation of membrane actuation for roll control of a micro air vehicle," *Journal of Aircraft*, **44** (*3*) 741–749 (2007). doi:10.2514/1.25356.
14) R.J. Bachmann, R. Vaidyanathan, F.J. Boria, J. Pluta, J. Kiihne, B.K. Taylor, R.H. Bledsoe, P.G. Ifju, and R.D. Quinn, "A Miniature Vehicle with Extended Aerial and Terrestrial Mobility," in: D. Floreano et al. (Ed.), Flying Insects and Robots, Springer Berlin Heidelberg, Berlin, Heidelberg, 2009: pp. 247–269. doi:10.1007/978-3-540-89393-6.
15) J.C. Gomez, and E. Garcia, "Morphing unmanned aerial vehicles," *Smart Materials and Structures*, **20** (*10*) 16 (2011). doi:10.1088/0964-1726/20/10/103001.
16) J.F. V Vincent, O.A. Bogatyreva, N.R. Bogatyrev, A. Bowyer, A. Pahl, and J.R.S. Interface, "Biomimetics : its practice and theory biomimetics : its practice and theory," *Interface*, 471–482 (2009). doi:10.1098/rsif.2006.0127.
17) A.Y.N. Sofla, S.A. Meguid, K.T. Tan, and W.K. Yeo, "Shape morphing of aircraft wing: status and challenges," *Materials and Design*, **31** 1284–1292 (2010). doi:10.1016/j.matdes.2009.09.011.
18) C. Thill, J. Etches, I. Bond, K. Potter, and P. Weaver, "Morphing skins," *The Aeronautical Journal*, (*3216*) 1–23 (2008).
19) A. Pelletier, T.J. Mueller, and N. Dame, "Low reynolds number aerodynamics of low-aspect-ratio , thin / flat / cambered-plate wings," *Journal Of Aircraft*, **37** (*5*) 825–832 (2000).
20) A.M. Halawa, B. Elhadidi, and S. Yoshida, "Aerodynamic performance enhancement using active flow control on du96-w-180 wind turbine airfoil," *Evergreen*, **5** (*1*) 16–24 (2018). doi:10.5109/1929723.
21) R.R. Harbig, J. Sheridan, and M.C. Thompson, "Reynolds number and aspect ratio effects on the leading-edge vortex for rotating insect wing planforms," *Journal of Fluid Mechanics*, **717** 166–192 (2013). doi:10.1017/jfm.2012.565.
22) N.I. Ismail, A. Zulkifli, R. Talib, H. Yusoff, and M.A. Tasin, "Vortex structure on twist-morphing micro air vehicle wings," *International Journal of Micro Air Vehicles*, **8** (*3*) 194–205 (2016). doi:10.1177/1756829316660321.
23) M.M. Takeyeldein, T.M. Lazim, N.A.R. Nik Mohd, I.S. Ishak, and E.A. Ali, "Wind turbine design using thin airfoil sd2030," *Evergreen*, **6** (*2*) 114–123 (2019). doi:10.5109/2321003.
24) M. Hwan, and J. Won, "Visualization and piv study of wing-tip vortices for three different tip configurations," *Aerospace Science and Technology*, **16** (*1*) 40–46 (2012). doi:10.1016/j.ast.2011.02.005.
25) N.I. Ismail, A.H. Zulkifl, M.Z. Abdullah, M.H. Basri, and N.S. Abdullah, "Computational aerodynamic analysis on perimeter reinforced (pr)-compliant wing," *Chinese Journal of Aeronautics*, **26** (*5*) 1093–1105 (2013). doi:10.1016/j.cja.2013.09.001.
26) N.A. Rahmat, A. Hagishima, N. Ikegaya, and J. Tanimoto, "Experimental study on effect of spires on the lateral nonuniformity of mean flow in a wind tunnel," *Evergreen*, **5** (*1*) 1–15 (2018). doi:10.5109/1929670.
27) S. Paulo, A. Maqsood, F.H. Huei, and T.H. Go, "Propeller-induced effects on the aerodynamics of a small unmanned aerial vehicle," *Journal of Aerospace Technology and Management*, **04** 475–480 (2012).
28) Z. Chen, "Micro Air Vehicle Design for Aerodynamic Performance and Flight Stability," PhD Thesis Dissertation, University of Sheffield, 2013.
29) I. Dynalloy, "Technical characteristics of flexinol ® actuator wires," 1–12 (2013). http://www.dynalloy.com/pdfs/TCF1140.pdf.
30) N.I. Ismail, a. H. Zulkifli, M.Z. Abdullah, M.H. Basri, and N.S. Abdullah, "Optimization of aerodynamic efficiency for twist morphing mav wing," *Chinese Journal of Aeronautics*, **27** (*3*) 475–487 (2014). doi:10.1016/j.cja.2014.04.017.
31) N.I. Ismail, A.H. Zulkifli, M.H. Basri, R.J. Talib, and M.M. Mahadzir, "Local angle of attack extraction method for twist morphing mav wing," *Jurnal Teknologi*, **75** (*8*) 37–41 (2015). doi:http://dx.doi.org/10.11113/jt.v75.5207.